City Research Online

City, University of London Institutional Repository

Graphical Abstract
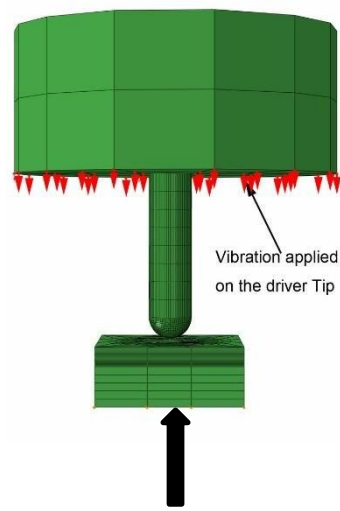
Vibration applied
on the driver Tip
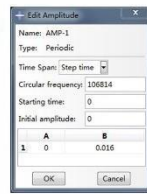
$$\sigma = [A + B\varepsilon^n][1 + C \ln \dot{\varepsilon}^*]$$

$$\varepsilon^f = [D_1 + D_2 \exp(D_3\sigma^*)][1 + D_4 ln\varepsilon^*][1 + D_5 T^*]$$

FE model with Johnson-Cook constitutive and fracture model
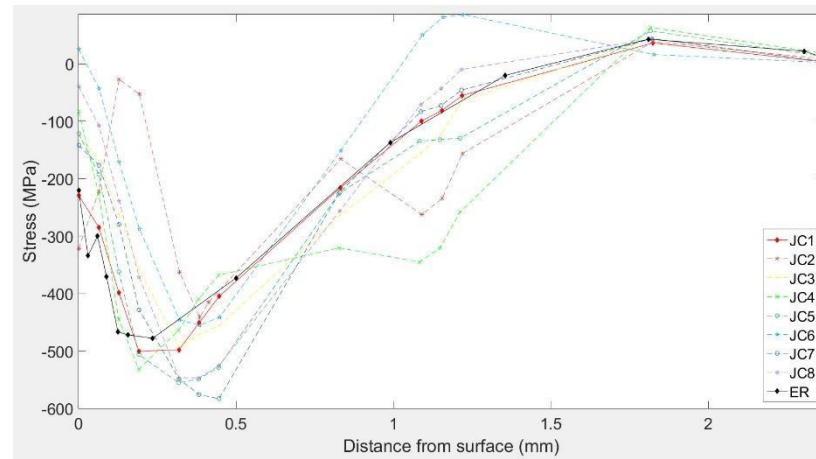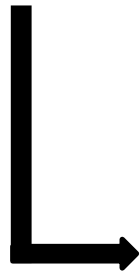
Influence of JC model parameters on peening residual stress
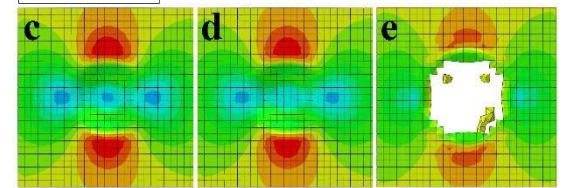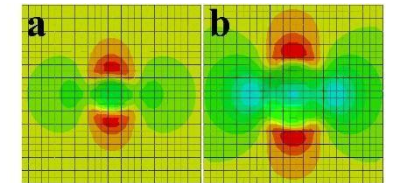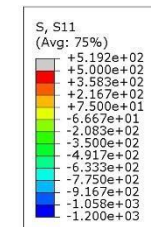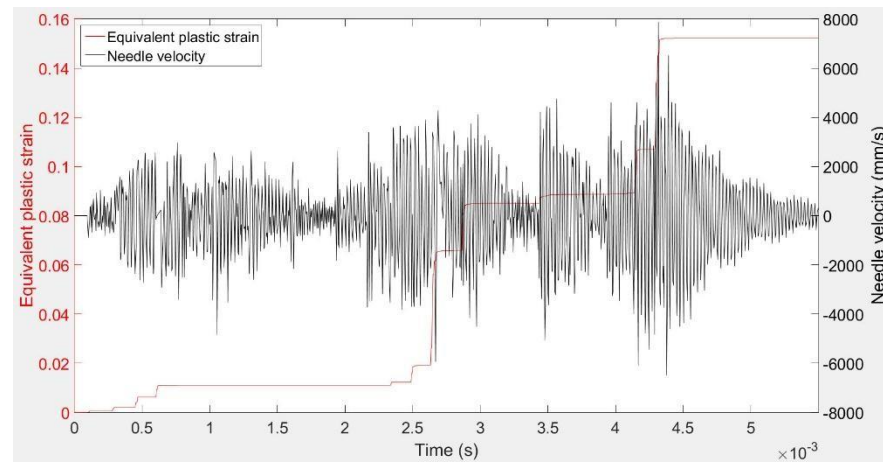
Fracture behaviour during long-duration peening

Development of a new 3D Model for the Prediction of Residual Stress and Fracture Behaviour in Ti-6Al-4V after Ultrasonic Peening Treatment

Danqing Yin[1,2], Dongpo Wang[3], Wuhui Li[1], Xiaojie Li[1], Heng Zhang[1], Sumsun Naher[2]

Abstract: Experimental and numerical studies have been carried out to determine the residual stress in Ti-6Al-4V after Ultrasonic Peening Treatment (UPT). Ultrasonic vibration output from the test equipment transducer was employed as the load to simulate the test conditions and the residual compressive stress in the material was measured by X-ray diffraction (XRD). A Johnson- Cook constitutive model was used to describe the rate-dependent stress-strain and failure behaviour of a sample. Based on motion analysis of the peening needle, a new 3D peen-rebound-peen (PRP) finite element model was developed to predict the stress field during and after the UPT process, using ABAQUS. The residual stresses predicted by the PRP model are in good agreement with the XRD results for the same peening and sample conditions. The effect of the gap width between the needle and the sample, the constitutive model parameters, and the peening duration were also studied.

Key words: Ultrasonic Peening, Ti-6Al-4V, Peen-rebound-peen model, Johnson-Cook Model, Residual stress, Fracture behaviour

1   Introduction

The Ultrasonic Peening Treatment (UPT) technique is a surface plastic deformation method that creates a peened metal surface by one or many metal needles, driven by a vibrating transducer, which, typically, works at a frequency of approximately 20KHz. By hitting the metal surface the UPT method produces a cold-hardened area on the metal. Hence, this method shares some common features with shot peening and hammer peening. However its high peening frequency alters its effects.

A typical example of commercial UPT equipment is shown in figure 1. This was developed by two of the current authors Danqing Yin, and Dongpo Wang, together with Ting Wang (2005). The digital power supply, controlled by a digital signal processer unit was developed by Ting Wang (2006). The half-wavelength handheld peening tool was designed in 2007 and described in detail by Danqing Yin (2010).

UPT can be applied in material processing, as a final step to generate a series of beneficial effects. Statnikov et al (2006) concluded that residual compressive stress, grain refinement, hardness, corrosion resistance and wear resistance had all been enhanced after UPT. Fatigue life can be improved and in some cases it can be increased by up to 10 times more than in non-UP treated surfaces. Wang et al (2003) stated that fatigue life had been extended 3 to 10 times longer than in Titanium alloy BT20 peened joints, using TIG welding, and 29 to 40 times longer than in the joints of the same material using electron beam welding. In the work of Abdullah et al (2012), fatigue life was

increased by 120% by 300 MPa peak to peak dynamic loading and the rate of increase was 70% in the 330 MPa dynamic loading range. Malaki and Ding (2015) found that up to an eightfold improvement in fatigue life could be obtained in critical welded parts by means of UPT.

Out of the many strain hardening processes for post-weld and strengthening treatments such as hammer peening, shot peening, laser peening and cavitation peening, ultrasonic peening (UP) is the most complex, due to the dynamic interaction between the indenter (the needle in ultrasonic peening) and its object, when tens of thousands of impacts occur every second. Accordingly, apart from investigation of its potential industrial applications, both experimental and analytical studies have been carried out to obtain a better understanding of the physical processes involved and to predict its effects. The major part of this effort has been in computer modelling. However, due to the highly dynamic and transient character of this process, it has only become possible with the development of high performance computers that provide fast enough numerical solutions.

~~There are many other strain hardening processes for post-weld and strengthening treatments such as the hammer peening, shot peening, laser peening and cavitation peening. Among these treatments UP may be the most complicated one in kinematics and interaction between the indenter and object. Duration of Each impact measured from hundreds of microseconds to units of milliseconds which means over tens of thousands of impacts occurs every second.~~ Complex microstructure transformation and both rate and temperature dependent phenomena, such as stress changes and high rate deformation, occur during this treatment. Accordingly, numerous efforts have been made to determine its stochastic nature. These have been mainly based on the use of commercial finite element code, using both 2D and 3D models. The indenter of the UP tool in these studies was modelled as a three dimensional (3D) rigid needle. Statnikov et al (2004) setup the indenter as a 3D needle and a sphere. Li et al (2012) also modeled the indenter as a needle. Guo et al (2015) established a 3D model with one or two rigid needles. Li (2009), used an orphan mesh to establish a 3D peening indenter. Mordyuk and Prokopenko (2006) used a cross-sectional shape for the indenter and setup a 2D model. Statnikovet et al (2004) applied a peening velocity to the indenter as the load. The relationship between the driving energy and the velocity was then determined. The results of all these studies, were almost similar and indicated that the maximum value and depth of the residual stress in the specimens increased significantly when the peening velocity was raised. The influence of velocity on the residual stress has been investigated along with other variables such as indenter diameter, the number of impacts during UP, the duration of the UP treatment and, the coverage of the peening. Li et al (2012) found that the diameter of the indenter has similar effects on the magnitude and depth of residual stress in the specimens. Yang et al (2012) also found that increasing the peening coverage resulted in increased depth of compressive residual stress but its maximum value decreased. Li also showed that by increasing the impact duration, the ultrasonic impact strengthening characteristic becomes more obvious and the depth of the compressive stress increases. Most of these investigations concentrated on simulating one or more impacts for the peening process, but ignored other complex phenomena associated with the real peening process. Mordyuk and Prokopenko (2006) studied the influence of rotating pin UPT on the fatigue behaviour of titanium samples. In these papers, the effects of multiple peening were not considered. Typically, Yang et al (2012, 2014) considered only one impact, while Li et al (2012) simulated only three impacts. Their models are time effective but ignore the progressive development of stress and strain in the specimens. Therefore, the aim of this study was to simulate the natural process of ultrasonic peening, including the practical effects of multiple steps of peening, peen-rebound-peen (PRP) processes of the indenter, progressive strain and stress and deformation.

1.1 Simulation of Peening Process

1.1.1 Theory of the PRP Model

The UP process is based on the impact between the driver, the needle and the specimen. Other than in the case of shot peening, the needle rebounds, after peening the metal surface with a certain velocity, and then comes in contact with the driver surface to acquire a new velocity. This velocity is determined by the residual kinetic energy in the needle, after the first peening and the new proportion of kinetic energy drawn from the driver. Kendal (1970) studied this process and described it in an equation as

where E_o is the maximum output energy from the driver, A is the transmission line cross-sectional area, u_0 is one-half of the peak-to-peak vibrational amplitude, E is the elastic modulus of the transmission line tip, L is the gap between mean position of the driver tip and the impact surface of the specimen.

This amount of energy is transferred to the needle as the kinetic energy that drives it. Then the gain in the needle initial velocity can be estimated as

where E_{kp1} is the initial kinetic peening energy and v_{p1} is the initial velocity of the needle. The velocity can then be determined by substituting equation (1) into (2) and the equation becomes

When the needle impacts the surface of the specimen this amount of energy E_{kp1} will be transferred to the specimen as the deformation energy. This deformation energy can be divided into two parts, namely: the elastic deformation energy and the plastic deformation energy. A new equation that describes this can be expressed as

where, E_{e1} is the elastic deformation energy and E_{p1} is the plastic deformation energy, = Material yield stress, is the Elastic strain, is the Plastic strain and V is the deformation volume of the peened area (assuming it is a cylinder).

The elastic energy E_{e1} can be expressed as

After dissipation of the plastic deformation energy, the needle gains its rebound kinetic energy from this amount of elastic deformation energy E_{e1} with a velocity determined by

where E_{kr1} is the rebound kinetic energy of the needle and v_{r1} is the rebound velocity of the needle. Note that $v_{r1} < v_{p1}$.

Assuming the driver tip and needle are hard enough not to deform plastically on their contact surfaces, it can be concluded that only elastic collision occurs on the contact surfaces. Due to vibration, the needle gains a further amount of energy when contacting the driver tip. After absorbing this further amount of kinetic energy the needle flows back to peen the specimen for the

second time. If the driver transfers its maximum amount of energy every time the needle contacts its tip then the kinetic energy for the second peening can be described as

where E_{kp2} is the second kinetic energy of the needle and is the second peening velocity of the needle, when the output energy is E_o.

Since the driver gains a certain amount of energy between 0 and E_o, depending on the time the needle is in contact with its tip, the total amount of kinetic energy for the second peening should be

where E'_0 is the actual output energy ($0<E'_0<E_0$), E'_{kp2} is the actual kinetic energy of the needle and is the second peening velocity of the needle when the output energy E'_0 varies with the vibrational amplitude.

If the peening velocity , , …, is high enough, additional, plastic deformation will occur or the kinetic energy of the needle will be entirely dissipated in elastic deformation of the specimen. This can be described by the following equation as:

The PRP model in this paper was established to simulate progressive deformation during peening and to predict the residual stress after peening using these equations.

1.1.2 Material constitutive and fracture model

Since the duration of one single peening is generally measured in units of microseconds or milliseconds, a rate-dependent constitutive model should be considered to describe the stress-strain relationship during UP. There are several models that predict the strain rate effect, often used in transient analysis. Cowper and Symonds (1958) studied the strain hardening and strain rate effects in the impact loading of cantilever beams and developed a strain-dependent constitutive model. Maier (1970) studied the piecewise linear constitutive laws with associated flow rules formulated in matrix notation. Zerilli and Armstrong (1987) modified the Cowper-Symonds model and updated it to a mixed piecewise linear model. The Johnson-Cook (1983) constitutive model includes both the effects of strain hardening and strain rate hardening during material deformation. The Johnson-Cook constitutive model is integrated in ABAQUS and can be easily used. Therefore this was employed for the simulation. Their equation as used in this model is expressed as

where ε is the equivalent plastic strain, is the dimensionless plastic strain rate with . A is the yield strength of the material at the reference strain rate at room temperature. B is the strain hardening constant, n is the strain hardening coefficient and C is the strain rate strengthening coefficient. The thermal term in the equation is not considered because thermal effects are negligible during ultrasonic peening at room temperature.

Johnson and Cook (1985) also studied the fracture behaviour of several materials based on an accumulative damage law, the damage to an element is defined as

where is the increment of equivalent plastic strain which occurs during a load cycle, and is the equivalent strain to fracture, under the current conditions of strain rate, pressure and equivalent stress. Fracture will occur when D = 1.0. The general expression for the strain at fracture is given as

2   Work Carried Out

2.1 The Test Rig and its Analytical Model

A 3D model using a C3D8R element, which is an 8-node linear brick, reduced integration, with hourglass control ability was established to simulate the experimental set-up of the UP processing system. The 3D model set-up is shown in figure 2 as compared to experimental set-up. Figure 2a shows the model set up and figures 2b-c show the mesh. The specimen was divided into 2 parts in depth during meshing (see, figure 2a). This part was divided into 20 layers. The thickness of each layer in the upper part was 75µm. So the dimensions of the smallest mesh in the specimen were 75µm×75µm×75µm. The dimensions of the needle were ϕ4mm×12mm and the specimen dimensions were 15mm×15mm×5mm. As shown in figure 2b, the meshing was divided into 3 parts on the treated surface namely, the inner part, the transient part and the outer part. The cell dimensions of the inner part were 75µm×75µm and this could represent changes in both strain and stress with sufficient, accuracy. The actual test rig used is shown in figure 2d. The material of the driver tip and the needle was 41Cr4 steel. Both were quenched and designed for ease of replacement if damaged during operation. To simplify simulation, only the driver was modelled as having the elastic property of steel while the needle was modelled as a rigid body.

2.2 Boundary Conditions and Load

The governing parameters of the PRP process were the driver's vibration amplitude and frequency. The amplitude was measured using an ultrasonic amplitude meter. The driving frequency was read directly from the LCD screen ultrasonic power supply. Studies have shown that the operational frequency of the transducer and the frequency of the indenter were not the same. Statnikov et al, (2006) found that during the UPT process, at least 75% of power, which was inherently small, was expended on unproductive processes other than peening. In Mordyuk and Prokopenkos' paper (2007) the vibration frequency and impaction frequency were 21KHz and 3KHz, respectively. Kudryavtsev et al (2010) also pointed out that the operational frequency of the transducer and the frequency of the intermediate element-striker were not the same. For this investigation, the peening frequency was determined by the driver's vibration frequency and the gap between the needle tip and the sample surface before peening. Details of this are given in sections 2.3 and 3.1. In figure 3, the parameter A represents the starting value of the vibration amplitude and parameter B represents the finishing value. The peening frequency input in this plane was the circular frequency and the relationship between frequency and circular frequency was shown as ω π , where ω is circular frequency or angular frequency, f is linear frequency. The vibration parameters of the driver were then set to 106814Hz of circular frequency and 16µm of vibration magnitude as shown in figure 3. These two parameters were input as the boundary conditions of the load module in ABAQUS.

In this PRP model, the needle pin was constrained in the x and y directions. The pin was only allowed to move in the z direction which is the peening direction, shown in Figure 3. The bottom surface of the sample was fixed in three directions to avoid any displacement during peening.

2.3 Peening frequency and gap set-up in model

The driving frequency was read directly from the LCD screen ultrasonic power supply while the peening frequency was estimated from measurements of the driver's frequency. It was concluded that the peening frequency is not greater than 25% of the vibration frequency.

It was noted that the applied pressure to the transducer had to be greater than a minimum value to ensure stabilisation of the peening and contact between the needle pin and the samples. The simulation model allowed for the gap width between the pin and the specimen to be varied in order to obtain agreement between the simulated and measured residual stresses. Four different gaps of 0.03, 0.38, 0.5 and 1.5mm were selected between the needle and the specimen, as shown in Figure 4. Because of the time taken to traverse this gap during the peen-rebound-peen the gap width could be adjusted to obtain agreement between the measured and estimated, peening frequency.

Starting from 0.03mm where the gap between the needle and the sample is just enough to ensure that there will be a peen—rebound-peen process, the remaining values were set assuming that 1.5mm represented the maximum gap width that would occur during peening.

2.4 Materials and constitutive model

The sample material used in this study was Ti-6Al-4V, the chemical composition of which is listed in table 1. This was obtained from Firm et al (1994) Materials Properties Handbook.

Table 1 Percentage Chemical composition of Ti-6Al-4V by mass

Ti	Al	V	C	H	Fe	N	Other
85.56-87.80	5.50-6.75	3.50-4.50	≤0.08	≤0.0125	≤0.50	≤0.05	≤0.30

As mentioned in the introduction, the parameters of the Johnson-Cook (JC) model were also studied in this paper. Eight groups of JC parameters were investigated, as obtained from the sources listed in table 2, in order is to investigate the influence of each of them and to get the best possible parameters for the materials used.

Table 2 Johnson-Cook Model Parameters for Ti-6Al-4V

JC No.	A (MPa)	B (MPa)	C	n		Ref.
1	782.7	498.4	0.028	0.28	10^{-5}	Lee and Lin, 1998
2	724.7	683.1	0.035	0.47	10^{-5}	Lee and Lin, 1998
3	910	870	0.02	0.68	10^{-3}	Yang et al, 2012
4	869.4	649.5	0.0093	0.3867	10^{-2}	Wang et al, 2015
5	859	640	0.000022	0.22	1	Wang et al, 2015
6	862.5	331.2	0.012	0.34	1	Meyer and Kleponis, 2001
7	997.9	653.1	0.0198	0.45	1	Meyer and Kleponis, 2001
8	1098	1092	0.014	0.93	1	Seo et al, 2005

The fracture behaviour, which Johnson and Cook described, was also integrated in ABAQUS in this model. D_1, D_2, D_3 and D_4 are the displacements at fracture and have been specified for this simulation for D_1 to D_4 to be: -0.09, 0.25, -0.50 and 0.014, respectively. These parameters were from Lesuer's work (2000) which studied the JC model parameters of Ti-6Al-4V Titanium and 2024-T3 Aluminum.

2.5 Experimental Set-up and peening parameters

The area and duration of a single-shot peening was first measured in order to determine the peening coverage and total peening duration. There are three stages during a single peening: first, the needle gains initial energy from the driver and flies to the sample surface; second, the needle peens the sample; third, the needle rebounds back to the driver and finishes the single peening process. The duration is the total time of the three stages. The single peening duration was derived from numerical simulation to be 2.8×10^{-4}s, as discussed in section 3.2. It was also estimated, from the FE model, that a single peening produces a dimple of 0.5mm diameter. For 100% coverage, peening must be carried out 500 times. Hence, since the specimen dimensions were 10mmx10mmx4mm the time required for complete coverage was (2.8×10^{-4}s × 500=) 0.14s. Since time is also required for the operator to move the handheld tool to cover the whole sample surface, it was decided to set the standard PRP duration for each test. Hence, 100% peening coverage in the experiment corresponds to one single peening on a single location in simulation. 200% peening coverage corresponds to peening twice, and so on and so forth.

The titanium alloy specimens were treated using different parameters during treatment. The standard peening parameters were 22µm vibration amplitude, 17KHz vibration frequency, and 100% coverage, respectively. Peening durations of 1.5×10^{-4}s, 4.25×10^{-4}s, 2.8×10^{-3}s, 3.95×10^{-3}s, 4.4×10^{-3}s and 5.6×10^{-3}s were chosen to compare their influence on residual stress in the samples.

Due to computing limitations, single location peening was analysed by computation, as shown in figure 5a. However, testing covered the entire sample surface, as shown in figure 5b. Therefore, it was necessary to find the equivalent approach of these two processes.

The OLYMPUS PMG3 optical microscope was used to take microstructure from the sample surface to 500µm in depth. The sample was treated by the parameters: 1.7A output current, 22µm vibration amplitude and 200% peening coverage after 160s treatment.

2.6 Comparison between estimated and measured Residual stress and area averaging

Residual stress in the specimen was measured by X-ray diffraction (XRD), which is recognised as a reliable and practical method. The strain in the crystal lattice was measured by this means and the associated residual stress was determined from the elastic constants, assuming a linear elastic distortion of the appropriate crystal lattice plane. The test for residual stress analysis by X-ray diffraction was based on British standard BS EN 15305: 2008. The samples were processed using electrolytic polishing of the metallographic specimens to peel off the surface materials in order to measure the residual stress in each layer in depth. The polishing process was based on ASTM standard: E1558-09. The value of 2θ was chosen as 142, following BS EN 15305:2008 for titanium alloy. Different XRD peaks were shown in Figure 6. In the experiment, an irradiated area of 1 x 1 mm was used for XRD measurement of the residual stress using a Brucker D8 XRD. In the simulation, the same area averaging of the calculated stress was assumed. The residual stress determined using x-ray diffraction, is the arithmetic average stress in the irradiated area of the X-ray beam. The measured residual stress from the XRD can be seen in section 3.3, figure 12.

Figure 6a showed the sample in the ψ = 0. The presence of a compressive stress, for example, in the sample resulted in a contraction of Poisson's ratio, changing the lattice spacing and the diffraction angle, 2θ. If the sample was then rotated through a certain angle ψ (Figure 6b), the residual stress present in the surface changed the lattice spacing over the stress-free state and increased 2θ.

Osman (2004) studied the measurement of residual stress using X-ray diffraction. (*This statement, appears to be redundant because, as written, it has no connection to the following sentences related to Bragg's Law. Either explain the connection or omit)* The basis of all XRD measurement is Bragg's law. According to the Bragg's law and the theory of elasticity, it can be concluded that stress value σ is proportional to the slope M between the diffraction angle 2θ and sin2ψ, that is

$$\underline{\hspace{4cm}} \quad (13)$$

$$\underline{\hspace{5cm}} \overline{\hspace{1cm}} \quad (14)$$

K is the stress constant,

$$\underline{\hspace{3cm}} \underline{\hspace{4cm}} \underline{\hspace{1cm}} \quad (15)$$

where,

E is elastic modulus

v is Poisson's ratio

Ψ is the angle between the normal of the sample and the normal of the diffracting plane

θ is the angular position of the diffraction lines according to Bragg's law

θ₀ is Bragg's angle with no stress. (*Note earlier comment on Notation)*

The test for residual stress analysis by X-ray diffraction was based on British standard BS EN 15305: 2008. The samples were processed using electrolytic polishing of metallographic specimens to peel.

In order to determine the area-average residual stress in the simulation model, all the nodes in three circle areas were selected with diameters of 1mm, 0.75mm, and 0.5mm, as shown in figure 7, to calculate the area-average stress in the FE model. As can be seen in figure 7, there were 15 layers of nodes along this path, for a specified diameter. For the 1mm diameter case, all nodes within that range on the surface layer were selected, as shown in figure 7b. The, arithmetic average stress of these nodes was then calculated. This process was repeated on 15 layers to get the area-average stress at the end. Area-average residual stress curves from the simulation were compared to XRD stress curves to validate the accuracy of the PRP model.

3 Results and Discussion

3.1 Microstructure of the peened sample

The microstructure of the peened sample was captured and is shown in Figure 8. As can be seen from figure 8(a), there are two different structures in the image: the substrate materials, which are not affected by impact energy, and the peened materials which are dominated by deformation twins. The scale of the crystals in the substrate materials area and the deformed materials area are almost the same which means grain refining could not be observed in this sample. From figure 8(a) and (b) it can be pointed out that most of the twins were distributed within the depth of 300μm under the surface and especially rich in 50μm to 200μm.

3.2 The influence of the gap between the needle and the specimen

During peening, there has to be a gap between the needle indenter and the specimen surface, because of the rebound of the handheld tool caused by the interaction forces between the sample and the needle indenter. As explained in section 2.3, a series of gaps was employed to study the peening frequency and the residual stress. A comparison between the frequencies of the driver and the needle for the selected gap widths is shown in figure 9. Figure 9a to 9d show needle displacement vs driver displacement curves simulated from various gap width values.

As can be seen from figure 9, the needle peening frequency decreases as the gap is increased. The ratio between the needle and the driver frequency decreases from 40:43 to 3:43. When the gap width was set to 0.38mm, the peening frequency was about 25% (11:43) of the driver output frequency. This corresponded with the value given in Statnikov and Mordyuk and Prokopenko's work.

Residual stress curves are shown in figure 10. As the gap was narrowed from 0.5mm to 0.03mm, both of the peak value and the depth of the compressive residual stress decreased. In the case of the 1.5mm gap, the magnitude and depth of the compressive stress were the smallest because only three impacts occurred. In the case of the 0.03mm gap, the maximum compressive residual stress was the largest of all four gap width cases. If the effect of this gap was neglected, then a false prediction of the final stress in the specimens would be inevitable. In the following sections, a 0.38mm gap width was used in the PRP model.

3.3 Influence of JC parameters and experimental validation on residual stress

The duration of a single peening referred to in section 2.5, was determined by counting the time span shown in figure 11. Then, the strain rate of the UP process was determined by calculating the result of strain variation for the duration of a single peening. The maximum strain rate of the peening process with 22μm vibration amplitude is $1636s^{-1}$. This strain rate was used to determine the rate-dependent properties of Ti-6Al-4V in simulation.

Eight groups of JC parameters were selected and compared, to decide the best group for further simulations. The peening duration used was 0.001s in this simulation. The corresponding experimental peening duration was 30s as discussed in section 2.5. All the parameters are listed in Table 2. A comparative study between these groups of parameters was carried out and discussed in this section. Temperature effects were not taken into consideration in this model. The experimental residual (ER) stress, obtained from the XRD curve is shown in figure 12 with simulated residual stress curves from these eight groups of JC parameters.

It can be concluded from figure 12 that residual stress results from JC parameters group one (JC1) conform most closely to the experimental results (ER). The offset of the surface layer residual stress on the JC1 curve obtained from the experimental result on the surface was 7MPa. The offset of the maximum compressive residual stress on the JC1 curve, obtained from the ER curve was 21MPa. The magnitude and depth of the compressive residual stress derived from the JC1 group also agreed well with the experimental results. Hence, the JC1 parameters were used in all further simulations.

3.4 The influence of peening duration on Residual Stress

The residual stress from each peening duration was simulated and plotted. The durations selected were $1.5x10^{-4}s$, $4.25x10^{-4}s$, $2.8x10^{-3}s$, $3.95x10^{-3}s$, $4.4x10^{-3}s$ and $5.6x10^{-3}s$. Stress curves, in the specimen, were extracted from the surface down to a depth of 2.5mm. These curves are shown in figure 13. The maximum compressive stress values were obtained at the end of each of these

durations. Along with the extension of peening time, the magnitude and depth of the compressive stress increased remarkably. There was a 74.8% increment in the magnitude of the maximum compressive residual stress and 172.4% increment in depth when comparing the results of the 1.5×10^{-4}s curve with those of the 5.6×10^{-3}s curve. Then, as peening time increased the increment trend slowed down, as can be observed from the figure.

As described in section 2.1, the needle velocity, corresponding to its kinetic energy, varies during peening. On the curve of the needle velocity in figure 11, not all of the impacts will contribute to the deformation of the materials. Deformation will be done only the by those with a velocity greater than the threshold/critical value which can introduce a stress sufficient to deform the metal. The threshold of the velocity depended on the strength of the metal being hardened after peening. This phenomenon can be deduced by studying the velocity-strain relationship during peening, as shown in Figure 11.

Each negative velocity represents one impact on the surface. It can be observed from figure 11 that the plastic strain increased whenever the velocity was higher than the threshold value. From 4.25×10^{-4}s to 2.8×10^{-3}s there was a short stabilised phase during which no plastic strain was observed. Then, along with the higher peening velocity, which resulted in kinetic energy above the threshold value, further plastic strain was observed on the strain curve, with associated plastic deformation. As can be seen from Figure 11, among all the impacts, there were 12 that were sufficiently efficient to cause plastic deformation during the process. Although the output energy from the UP power supply was kept constant due to this process, UP produced more plastic strain as the sample surface got strain hardened during the processing.

3.5 Fracture behaviour simulated in PRP model

The recommended peening duration is only rarely mentioned in recent published works, although the peening duration and its influence have been studied since UPT was invented. In Yekta's (2013) study on proper, under- and over-treatment by UPT, recommendations were made by identifying the indent depth and flaking during operation. In this section, deformation and fracture behaviour under very long time peening will be discussed and proper peening duration will be recommended using PRP model as another approach of identifying under- and over-treatment of UP process.

From Wang's (2008) paper, it can be calculated that the compressive limit at breaking of Ti-6Al-4V is 8% when the strain rate is 1600s^{-1} while the strain rate during UP simulation is 1636s^{-1} based on the explanation in section 3.2. When all the parameters were input to ABAQUS, fracture behaviour into was tken into account during the simulation.

It can be seen from figure 14 that the first ten impacts only caused two periods of significant plastic strain. As can be seen from these figures, subsequent remarkable plastic strain was observed after 3.95×10^{-3}s. From 3.95×10^{-3}s to 5.6×10^{-3}s, although the magnitude and depth of the compressive stress kept increasing, as shown in figure 12, the residual stress field changed only slightly on the sample surface, as can be seen on the stress contour in Figure 14, until 5.6×10^{-3}s fracture was observed. In Yekta's (2013) paper, peening flaking was observed and over-peen behaviour has been studied. This model can give an insight into the progressive process of peening fracture and time.

The residual stress and fracture for different peening durations can be seen in figure 14. Based on the discussions in section 3.2, the simulated peening (SP) duration, UPT duration and peening coverage are listed in table 3.

Table 3 Relationship between SP durations and real UPT

Duration No.	a	b	c	d	e

SP duration	1.5×10^{-4}s	4.25×10^{-4}s	3.95×10^{-3}s	4.4×10^{-3}s	5.6×10^{-3}s
UPT duration	240s	360s	420s	450s	≈495s
Peening coverage	800%	1200%	1400%	1500%	≈1650%

As can be concluded from Figure 14 and Table 3, after 240s treatment, the residual stress fields on the sample surface kept stable. When treated to 495s, the magnitude of the residual stress exceeds the ultimate compressive value of the material. Stress significantly increases only in the depth direction. Hence, UP treatment should be carried out for no more than 800% coverage or the treatment will be disadvantageous to the materials. Although 1000% or more coverage is not commonly seen in surface hardening of substrate materials, operators intended to over-peen the weld seams to get better treatment results and remove a quantity of tensile residual stress by UP.

In this paper, the authors developed a new model to reproduce the multi-times peening process different from the one-shot peening models from other scholars. Certain pressure should be applied to ensure the stabilization of the peening process and contact between needle and samples but this pressure is uncertain when operated manually. Therefore, in this paper, the pressure applied by the operator would be unknown and considered consistent and was ignored during model set-up. As shown in the manuscript, an adjustable gap has been provided with width to ensure the accuracy of the simulated residual stresses will agree with the experience results. These are also discussed in the manuscript in details in different cases. In future works authors aims at measuring this pressure by fixing the handheld tool on a robot. In the current work the authors' aim is to present a new model which is better than the simple one-shot peening model with a fixed initial velocity.

4   Conclusions

A new 3D peen-rebound-peen model was developed in this paper which is capable of simulating the real peening process during UPT. Energy transformation and dissipation during this process were discussed. Based on this discussion it can be concluded that the kinetic energy of the needle indenter increased due to the PRP process. As XRD results were measured after area arithmetic averaging processing, the same averaging data process has been carried out on all the simulated residual stress results to ensure the same prediction accuracy.

Different gaps widths, set between the needle tip and the sample, have been studied to determine the difference between the driving frequency and peening frequency in the PRP model. A 0.38mm gap width was shown to be the best value. Material dynamic mechanical properties are vital to this simulation. The widely used Johnson-Cook stress-strain relationship model and fracture model were employed in the simulation and included in ABAQUS. From the eight groups of JC stress-strain model parameters selected, one group was chosen to be the best validated by the experimental results from the XRD. Along with extension of peening duration both the magnitude and the depth of the compressive stress in the peened sample were increased. This showed a beneficial trend for the use of this process in this material to achieve better final properties. Then Studies on peening duration and fracture behaviour of long-time peening were also carried out, based on the JC fracture model in this paper. It was found that as peening continued after 800% coverage, the surface compressive stress barely changed, while the risk of fracture increased. When peening coverage exceeded 1600% (5.6×10^{-3}s peening in simulation) a fracture was observed in the PRP model. In some fracture sensitive applications, when applying UPT to materials in a corrosive environment, high peening coverage needs to be avoided. Based on these studies 300%~400% peening coverage is recommended.

Acknowledgements

Reference

Abdullah A., Malaki M., Eskandari A., Strength enhancement of the welded structures by ultrasonic peening. *Mater. Des.* 38, 7–18, 2012.

Cowper G.R., Symonds P.S., Strain hardening and strain rate effects in the impact loading of cantilever beams, Brown Univ. Applied Mathematics Report, p28, 1958.

Firm K., Boyer R. and Welsch G., Materials properties handbook: Titanium Alloys. *ASM Int. Mater. Park. OH* xxii 1176, 1994.

Guo C., Wang Z., Wang D., Hu S., Numerical analysis of the residual stress in ultrasonic impact treatment process with single-impact and two-impact models. *Appl. Surf. Sci.* 347, 596–601 (2015).

Johnson G.R., Cook W.H., A constitutive model and data for metals subjected to large strains, high strain rates and high temperatures, 7th International Symposium on Ballistics, 541-547, 1983

Johnson G. R., Cook W. H., Fracture characteristics of three metals subjected to various strains, strain rates, temperatures and pressures. *Eng. Fract. Mech.* 21, 31–48, 1985.

Kendal L.A., Sonic impact metal deformation [Doctoral dissertation]. The Ohio State University, 1970.

Kudryavtsev Y., Kleiman J., Lobanov L., Knysh V., Prokopenko G., Fatigue Life Improvement of Welded Elements by Ultrasonic Peening. IIW Document XIII-2010-04, 2010.

Lee W.S., Lin C.F., Plastic deformation and fracture behaviour of Ti–6Al–4V alloy loaded with high strain rate under various temperatures. Mater Sci Eng A; 241: 48–59, 1998.

Lee W.S., Lin C.F., High-temperature deformation behaviour of Ti6Al4V alloy evaluated by high strain-rate com- pression tests. J Mater Process Technol 1998; 75: 127–136, 1998.

Lesuer D.R., Experimental investigations of material models for ti-6al-4v titanium and 2024-t3 aluminum. U.S. Department of Transportation/Federal Aviation Administration, DTFA03–97Z-90007, 2000.

Li Jin-yi, Ling X., Zhou J., Finite element simulation of residual stress field induced by ultrasonic impact treatment. *J. Aeronatical Mater.* 32, 84–88, 2012.

Li T., Numerical simulation of ultrasonic impact treatment on welding residual stress [Master's Dissertation]. Harbin Insititute of Technology, 2009.

Maier G., A matrix structural theory of piecewise linear elastoplasticity with interacting yield planes. *Meccanica* 5, 54–66, 1970.

Malaki M., Ding H., A review of ultrasonic peening treatment. *Mater. Des.* 87, 1072–1086, 2015.

Meyer H.W., Kleponis D.S., Modeling the high strain rate behavior of titanium undergoing ballistic impact and penetration. Int J Impact Eng, 26: 509–521. 2001.

Mordyuk B.N., Prokopenko G.I., Fatigue life improvement of α-titanium by novel ultrasonically assisted technique. *Mater. Sci. Eng. A* 437, 396–405, 2006.

Mordyuk B. N., Prokopenko G. I., Ultrasonic impact peening for the surface properties' management. *J. Sound Vib.* 308, 855–866, 2007.

Osman A., Residual stress measurement using X-ray diffraction [Mater's Dissertation]. Texas A&M University, 2004.

Seo S.W., Min O.K. and Yang H.M., Constitutive equation for Ti-6Al-4Vat high temperaturesmeasured using the SHPBtechnique. Int J Impact Eng 31(6):735–754, 2005.

Statnikov E. S., Korolkov O. V., Vityazev V. N., Physics and mechanism of ultrasonic impact. *Ultrasonics* 44, e533–e538, 2006.

Statnikov E., Korolkov O.V., Vityazev V. N., Physics and mechanism of ultrasonic impact treatment. IIW Document XIII-2004-04, 2004.

Wang T, Research on the development of digitalised ultrasonic peening power supply using DSP chip, Tianjin: Tianjin University, 2006.

Wang DP, Huo LX, Zhang YF, Improvement of fatigue properties of welded joints for titanium alloy by ultrasonic peening method. *Chinese J. Nonferrous Met.* Vol. 13, 1456–1460, 2003.

Wang F., Zhao J., Zhu N. and Li Z., A comparative study on Johnson – Cook constitutive modeling for Ti – 6Al – 4V alloy using automated ball indentation (ABI) technique. *J. Alloys Compd.* 633, 220–228, 2015.

Wang X.F, Lu F.Y and Lin Y.L., Study on dynamic mechanical characteristics of TC4 titanium. in *5th* National *Comference on mechanics of explosion* 230–236, 2008.

Yang S.B., Xu J., Fu Y., and Wei W., Finite element modeling of machining of hydrogenated Ti-6Al-4V alloy. *Int. J. Adv. Manuf. Technol.* 59, 253–261, 2012.

Yang X., Zhou J., Ling X., Study on plastic damage of AISI 304 stainless steel induced by ultrasonic impact treatment. *Mater. Des.* 36, 477–481, 2012.

Yang X., Ling X., , Zhou J., Simulation of surface modification of S30403 stainless steel treated by ultrasonic impact treatment. *J. Nanjing Tech Univ.* 36, 28–34, 2014.

Yekta R.T., Ghahremani K. and Walbridge S., Effect of quality control parameter variations on the fatigue performance of ultrasonic impact treated welds. *Int. J. Fatigue* 55, 245–256, 2013.

Yin D.Q, Research on some aspects of welded joints properties improvement method of ultrasonic peening treatement, Tianjin: Tianjin University, 2010.

Zerilli F.J., Armstrong R.W., , Dislocation-mechanics-based constitutive relations for material dynamics calculations, Journal of Applied Physics, Vol. 61, No. 5, p. 1816-1825, 1987.

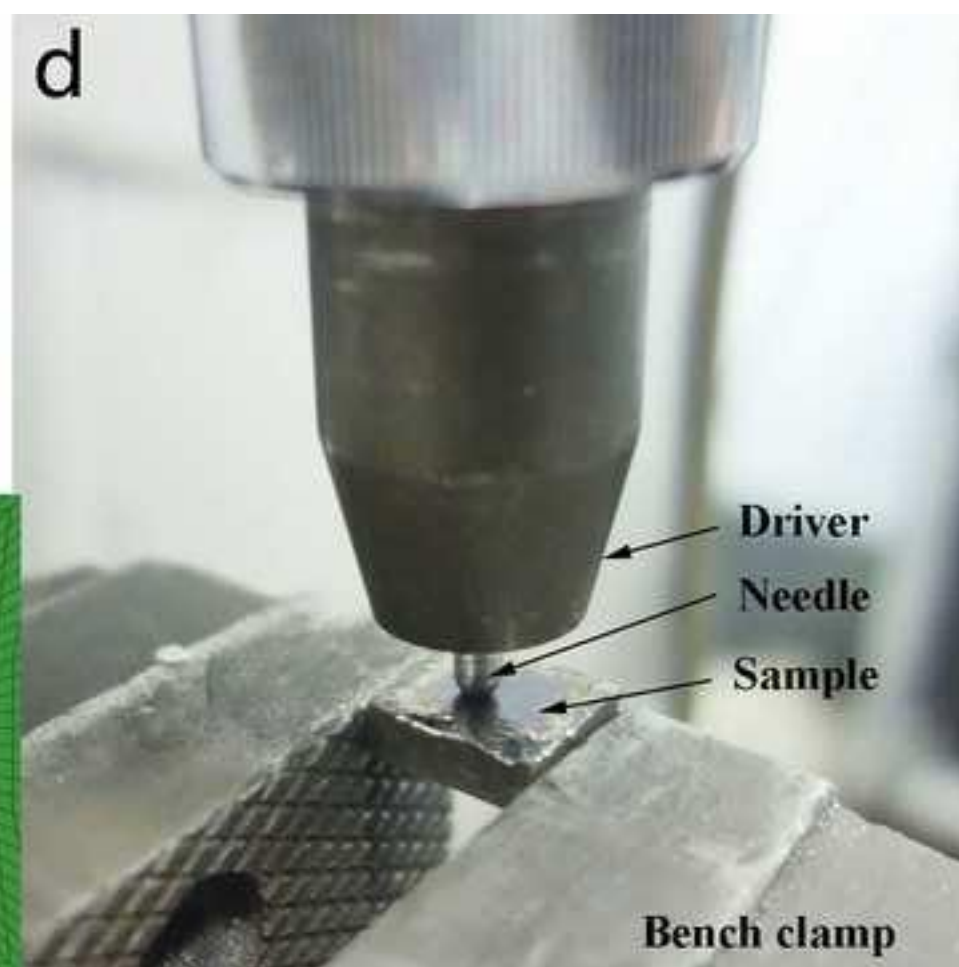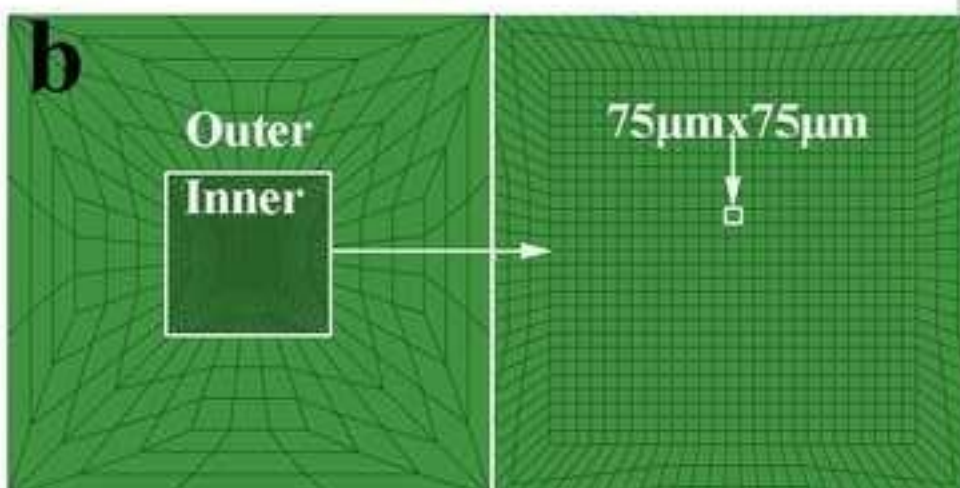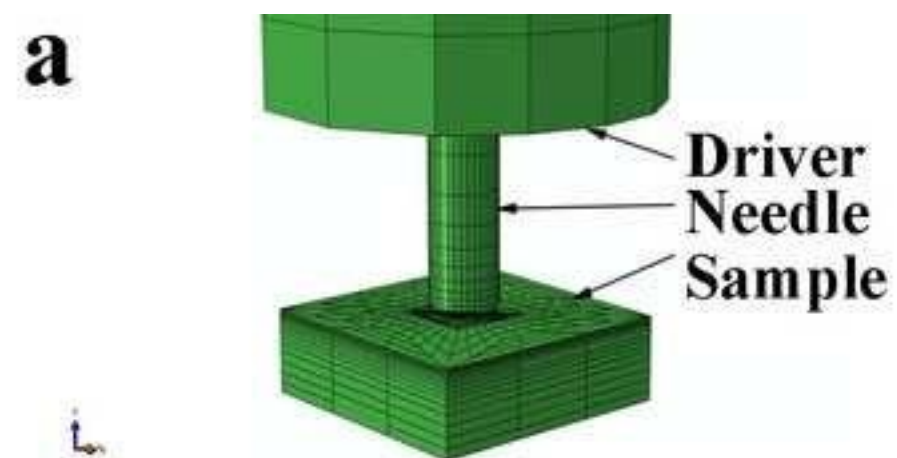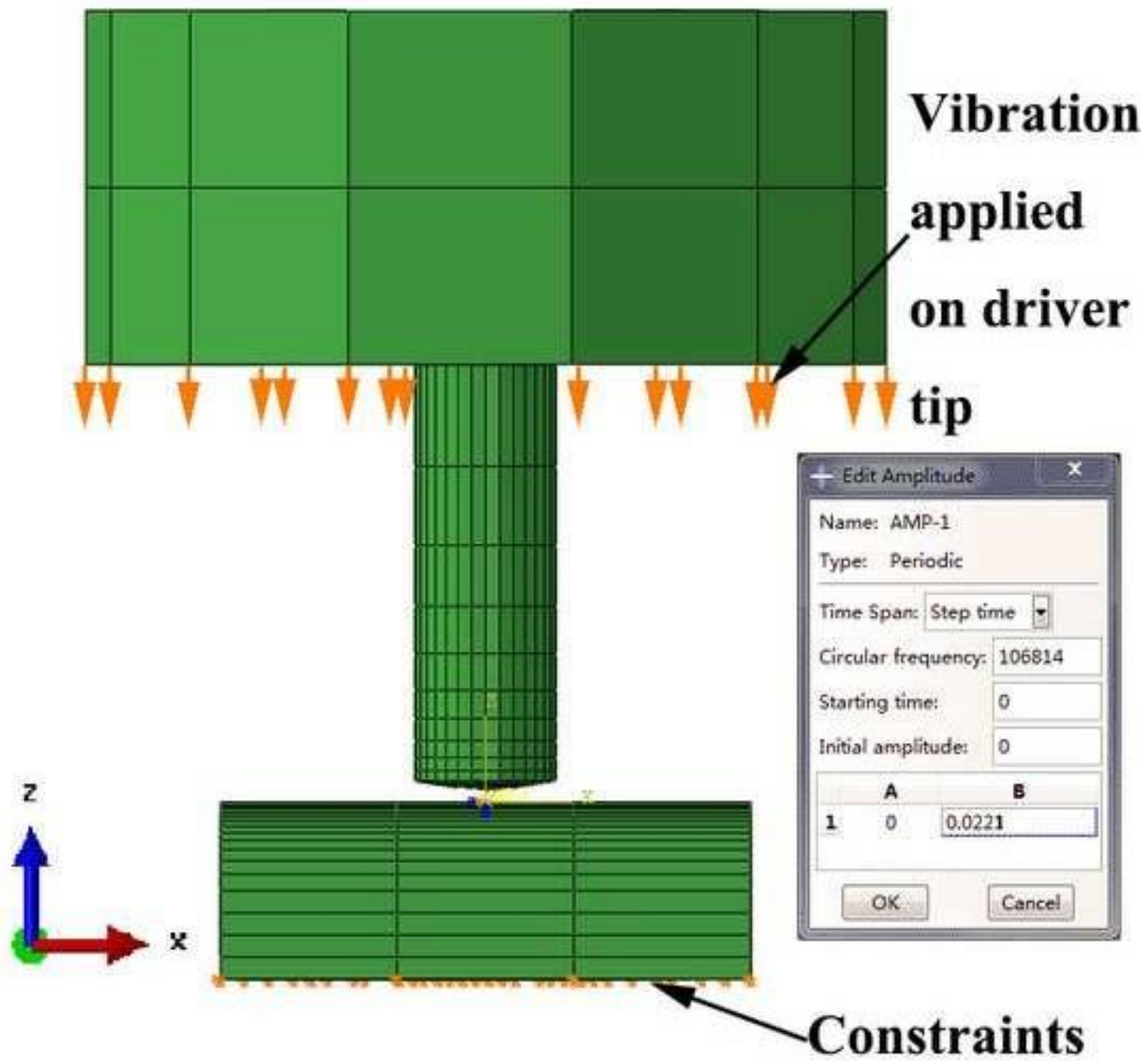**Figure1**
[Click here to download high resolution image](#)

Peening tip
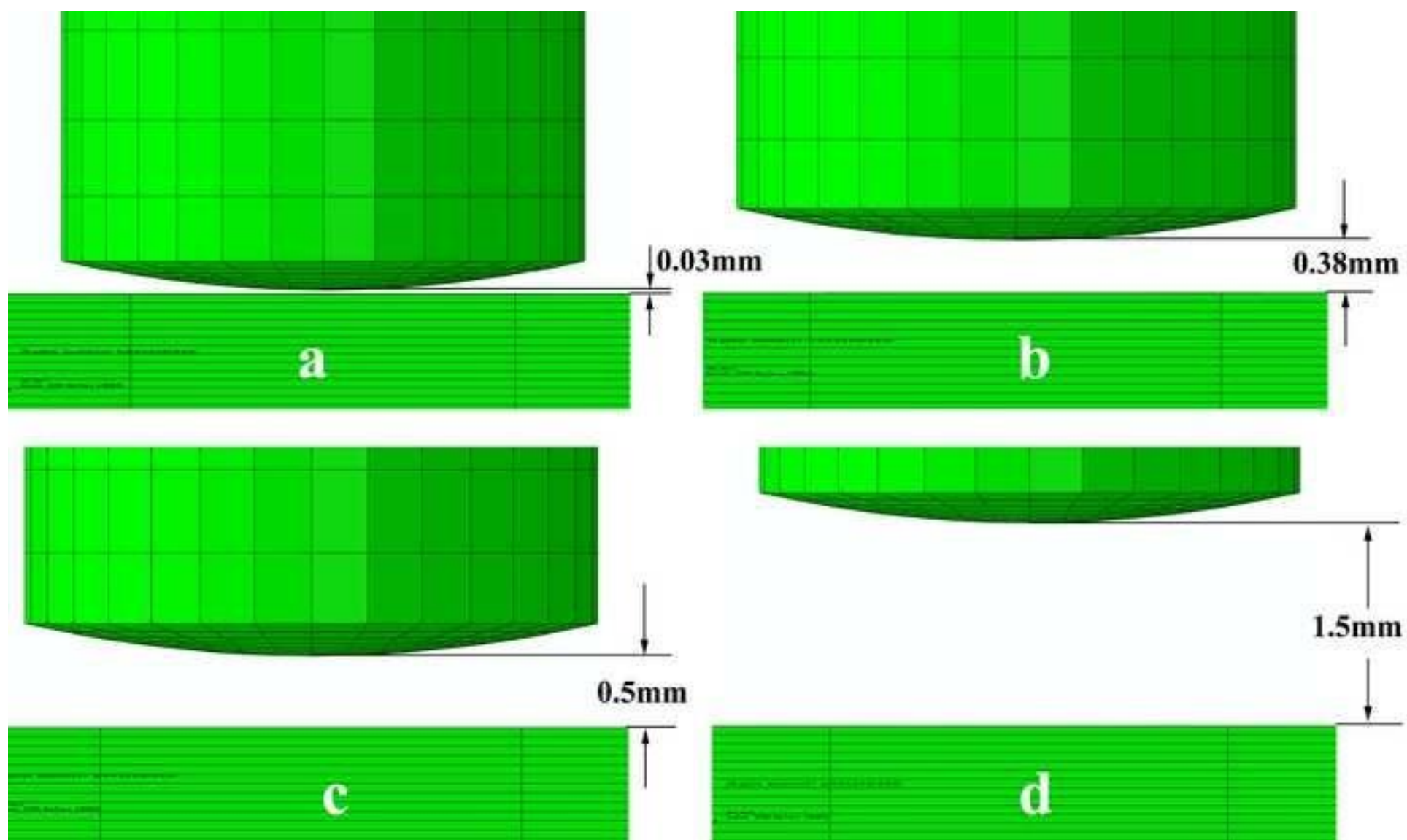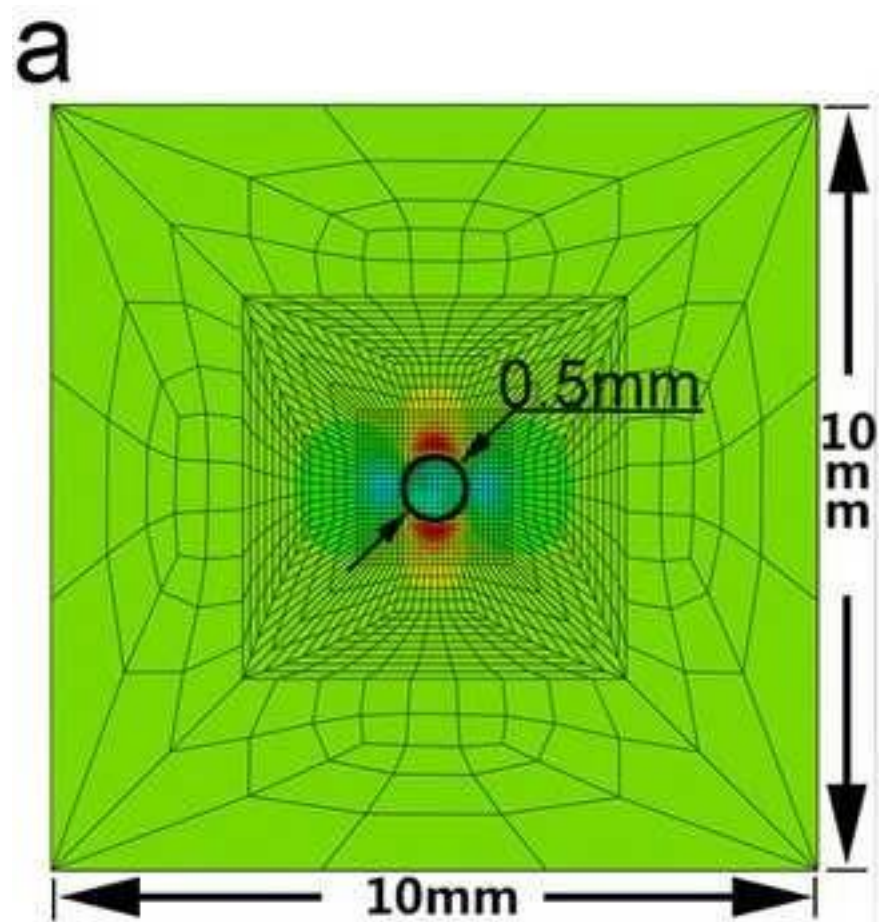
Power input

Handle

HJ-III型超声冲击机

ULTRASONIC PEENING TREATMENT EQUIPMENT

min   max

On

Run

Current

Display

Made in China
Tianjin University

Output

a

Driver
Needle
Sample

b

Outer
Inner

75μmx75μm

d

Driver
Needle
Sample

Bench clamp

Figure3
Click here to download high resolution image

0.03mm

0.38mm

a

b

0.5mm

1.5mm

c

d
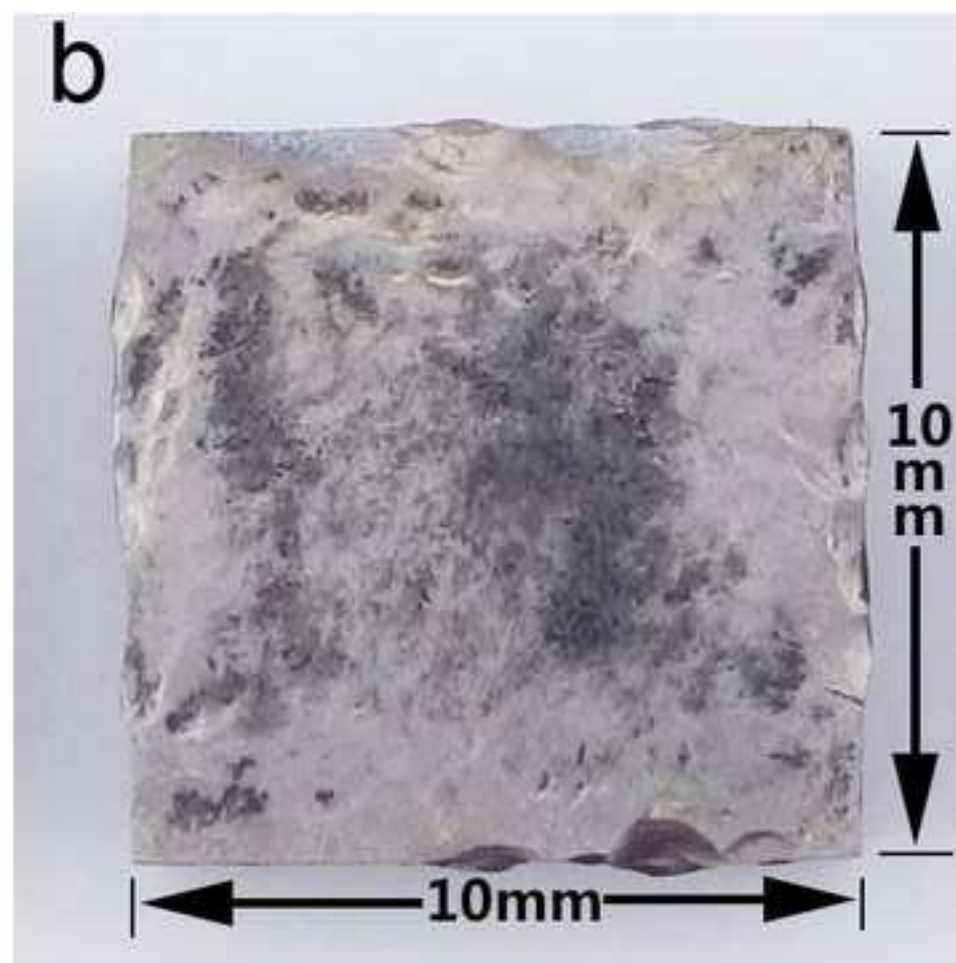
Figure5
[Click here to download high resolution image](#)
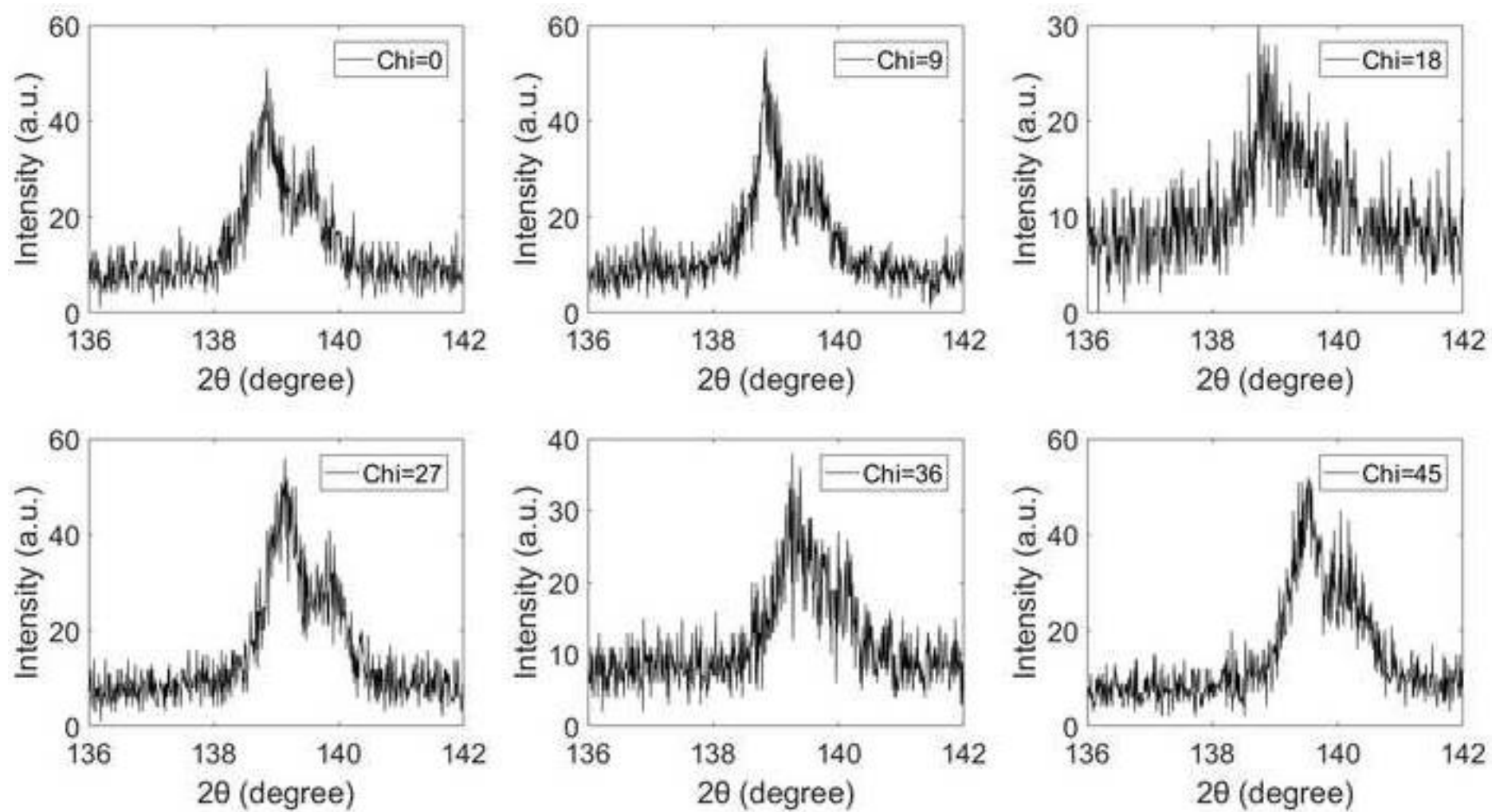
Figure7
[Click here to download high resolution image](#)
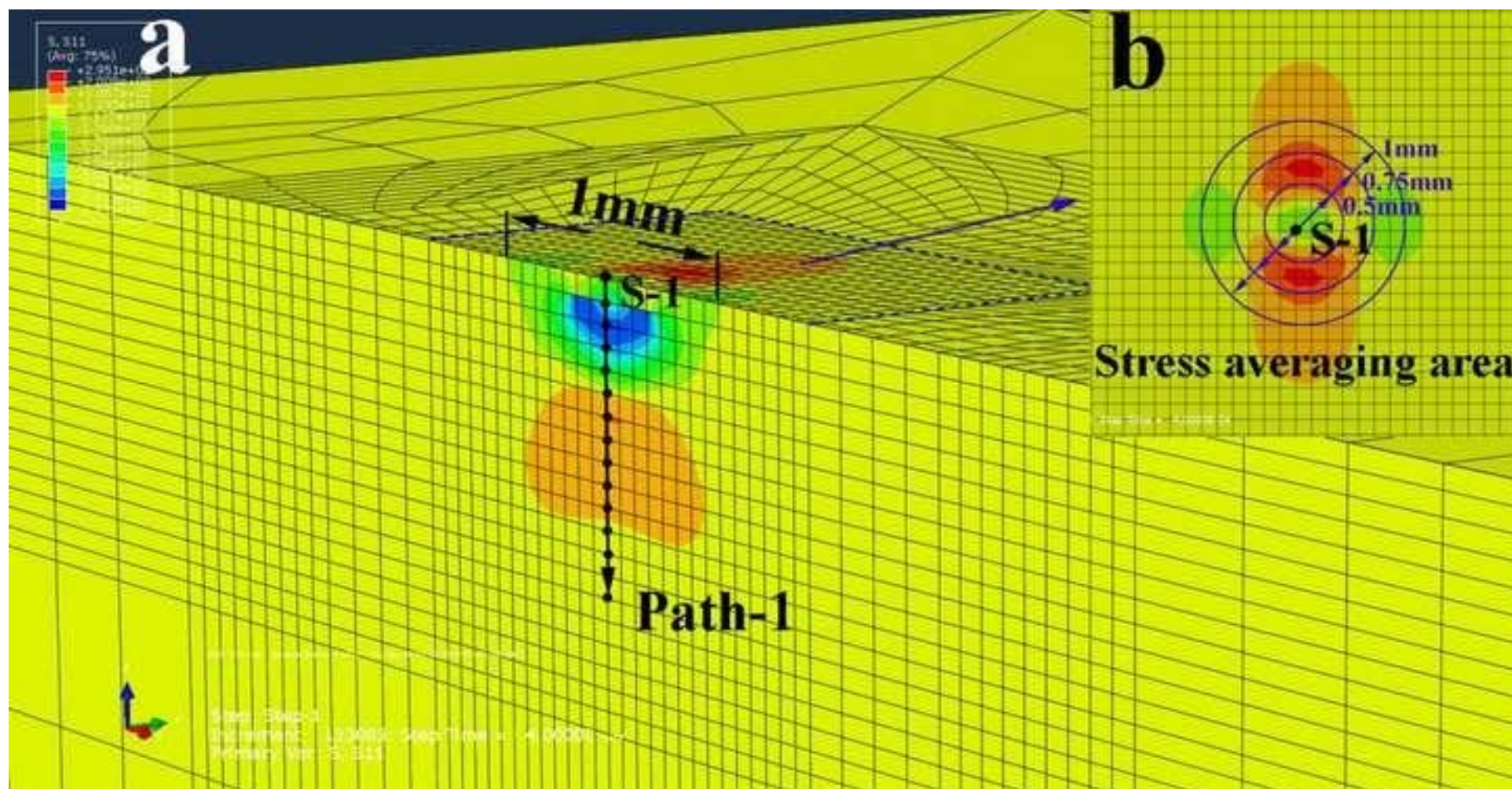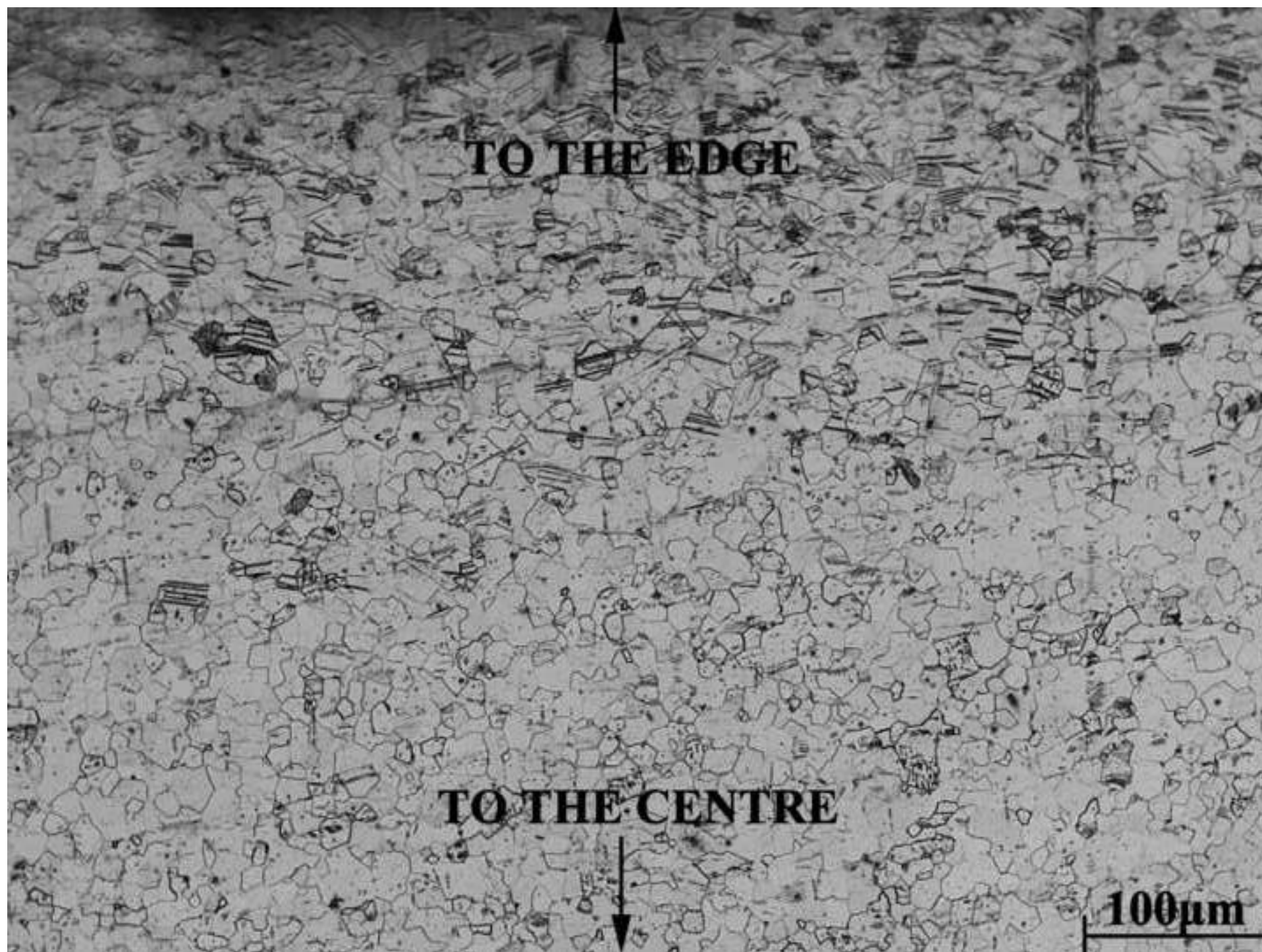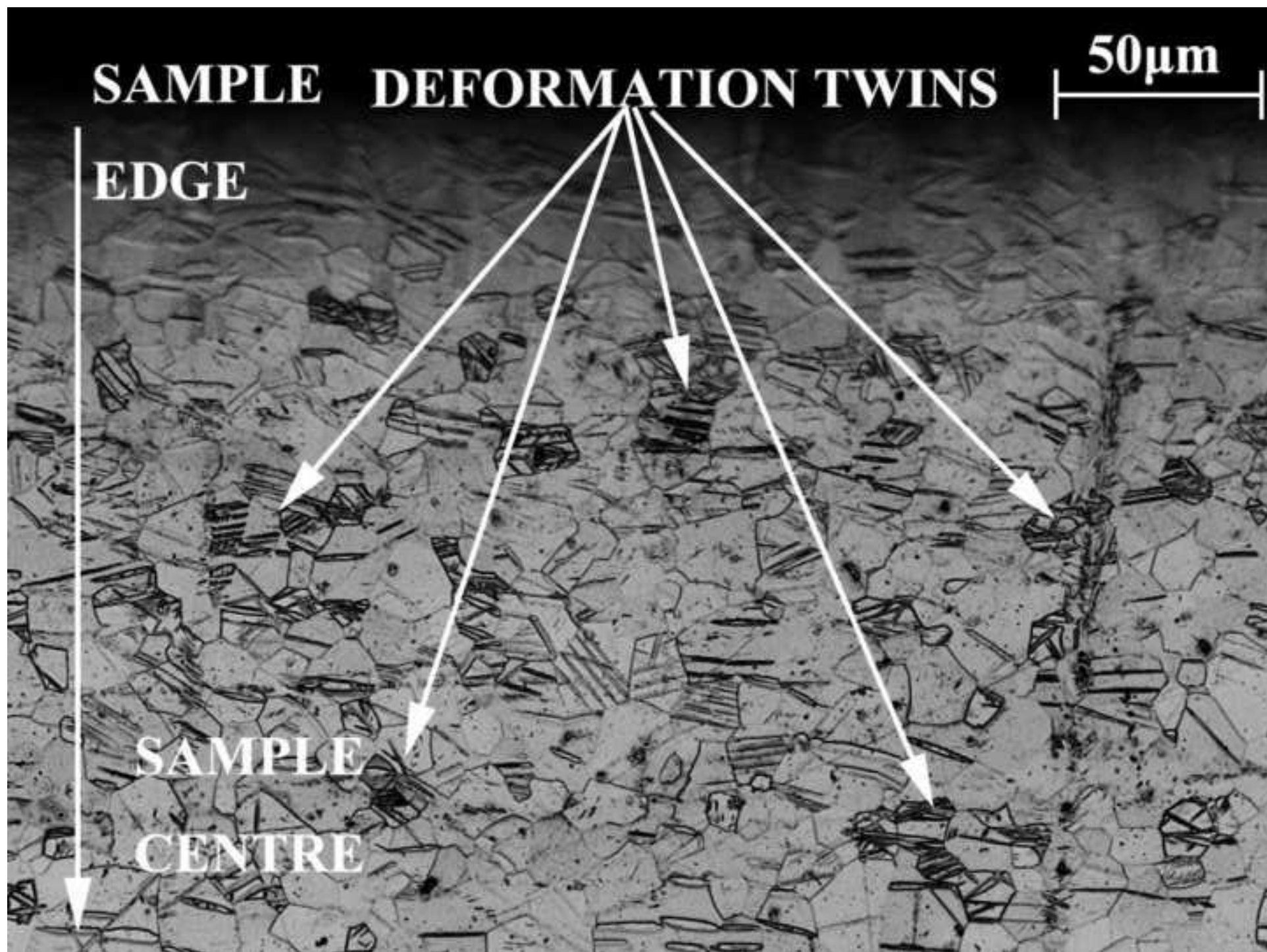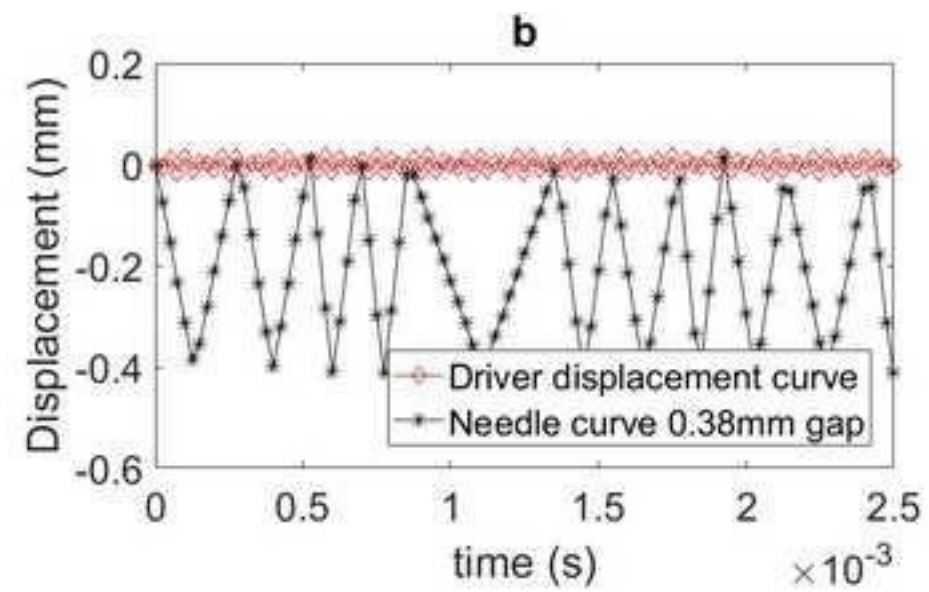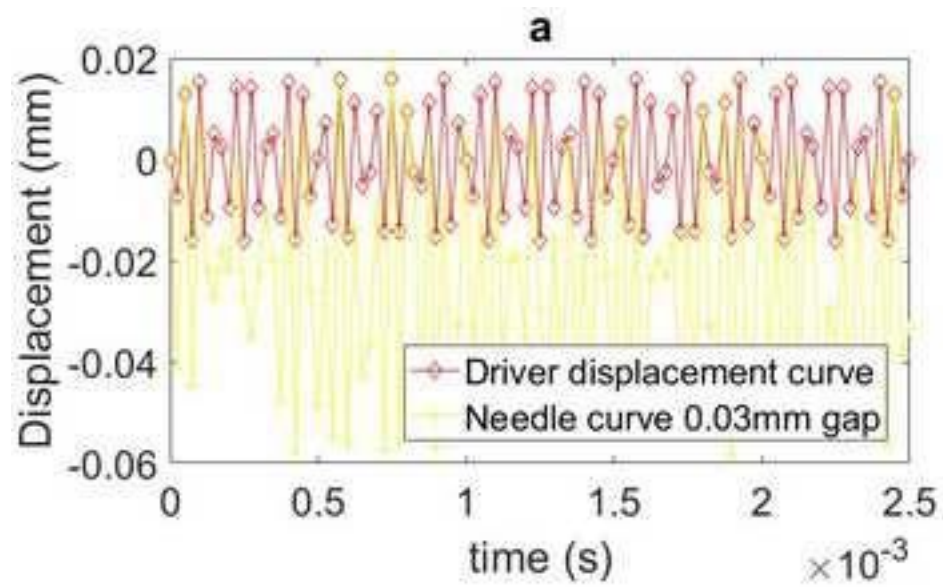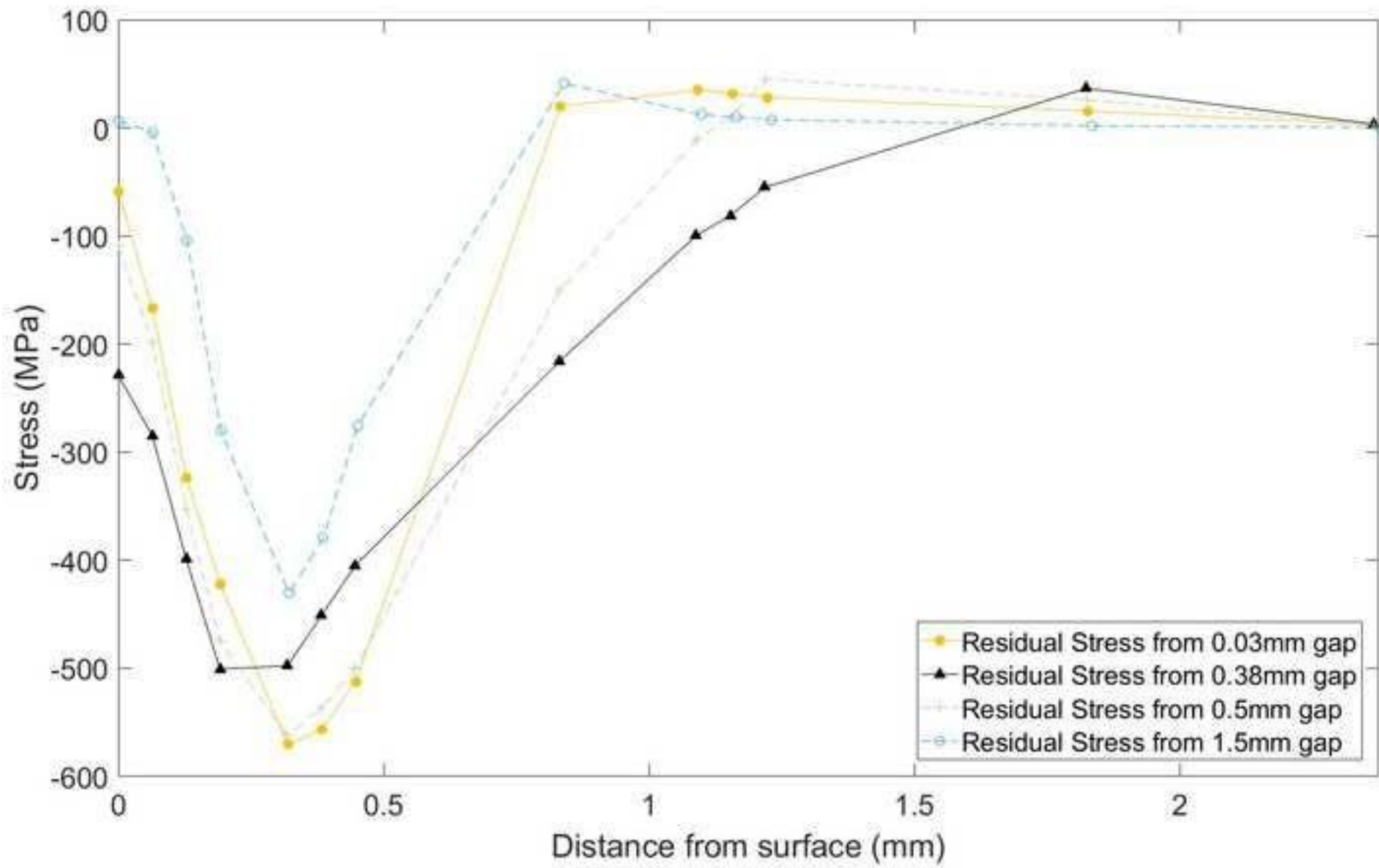
Figure9
[Click here to download high resolution image](#)
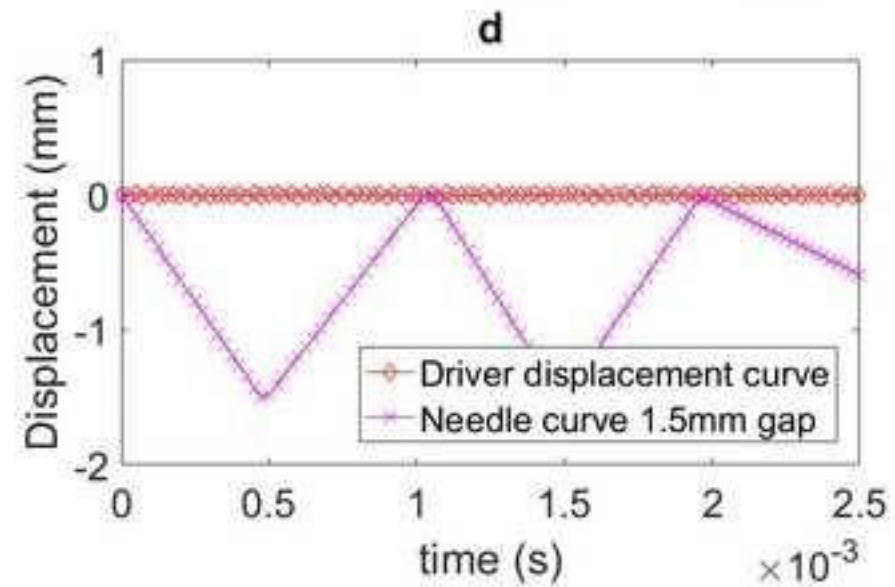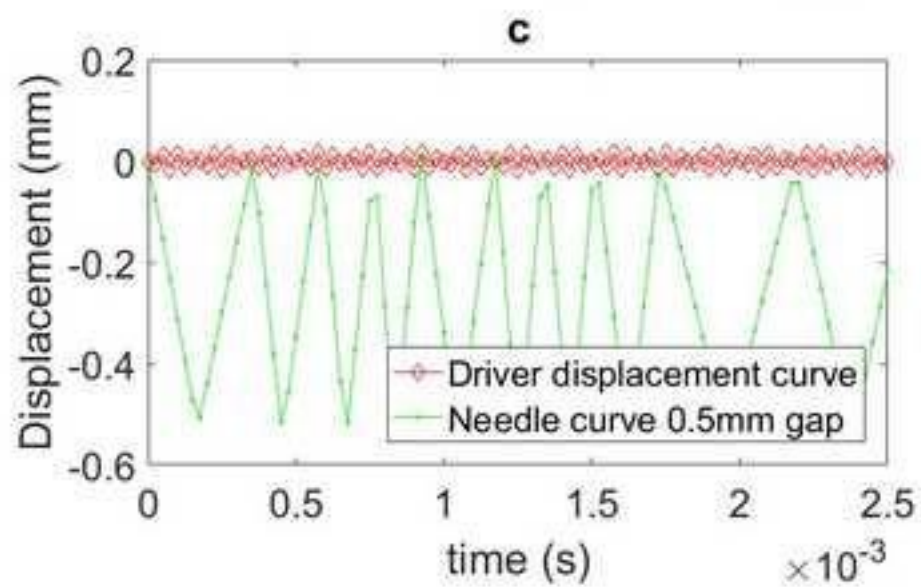
Figure10
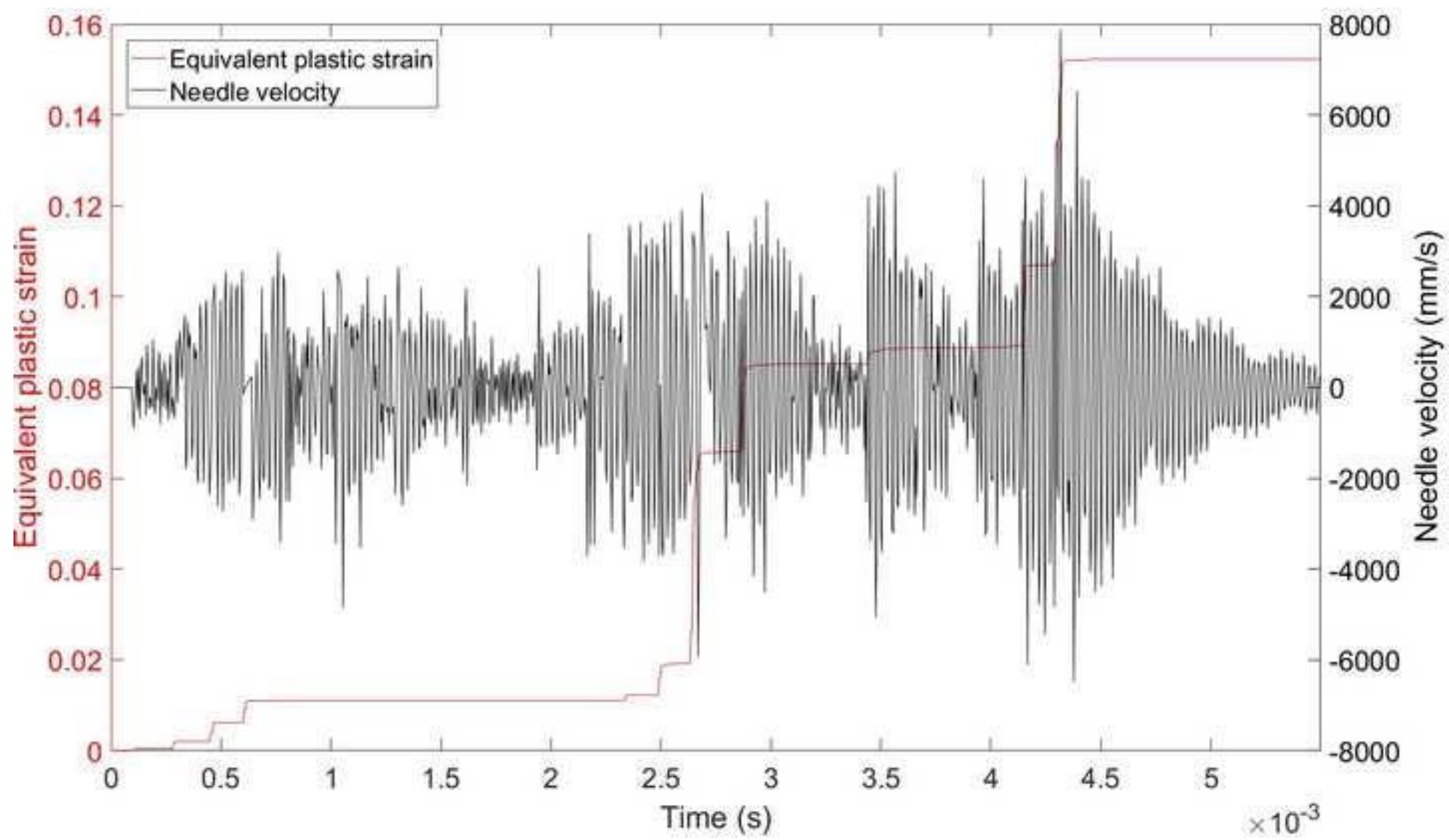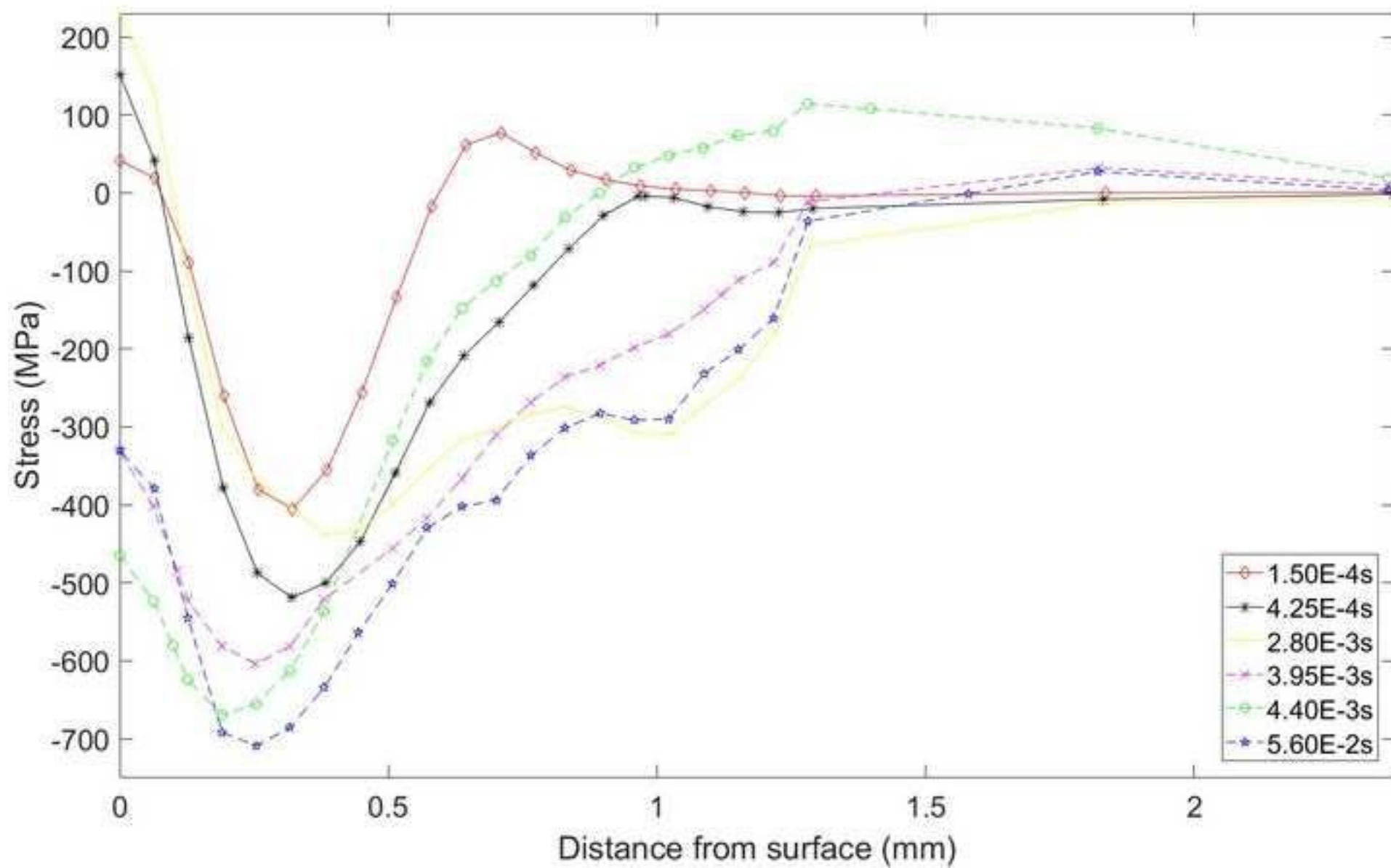[Click here to download high resolution image](#)

Figure11
[Click here to download high resolution image](#)

S, S11
(Avg: 75%)
+5.192e+02
+5.000e+02
+3.583e+02
+2.167e+02
+7.500e+01
-6.667e+01
-2.083e+02
-3.500e+02
-4.917e+02
-6.333e+02
-7.750e+02
-9.167e+02
-1.058e+03
-1.200e+03

a — Step Time=1.50E-4s

b — Step time= 4.25E-4s

c — Step Time=3.95E-3s

d — Step Time=4.40E-3s

e — Step Time=5.60E-3s